NASA CR-72373

LIQUID DROPLET EVAPORATION IN STAGNANT HIGH PRESSURE AND HIGH TEMPERATURE ENVIRONMENT

by

T. P. Torda and Robert Matlosz

prepared for

NATIONAL AERONAUTICS AND SPACE ADMINISTRATION
CONTRACT NGR 14-004-006

May 1968

Illinois Institute of Technology
Department of
Mechanical and Aerospace Engineering
Chicago, Illinois

NASA CR-72373

FINAL REPORT

LIQUID DROPLET EVAPORATION IN STAGNANT HIGH PRESSURE AND HIGH TEMPERATURE ENVIRONMENT

by

T. P. Torda and Robert Matlosz

prepared for

NATIONAL AERONAUTICS AND SPACE ADMINISTRATION

May 1968

CONTRACT NGR 14-004-006

Technical Management
NASA Lewis Research Center
Cleveland, Ohio
Chemistry and Energy Conversion Division
Robert D. Ingebo

ILLINOIS INSTITUTE OF TECHNOLOGY

Department of

Mechanical and Aerospace Engineering

Chicago, Illinois

TABLE OF CONTENTS

LIST OF TABLES

LIST OF ILLUSTRATIONS

LIQUID DROPLET EVAPORATION IN STAGNANT HIGH PRESSURE AND HIGH TEMPERATURE ENVIRONMENT

by

T. P. Torda and Robert Matlosz

ABSTRACT

The purpose of this research is the investigation of experimental vaporization histories for liquid droplets vaporizing in a subcritical, critical, and supercritical environment. Experimental vaporization histories have been obtained for 1800μ diameter n-Pentane drops vaporizing in nitrogen gas environment. The gas environment temperature was 850°R and the environmental gas pressure was varied from 200psi to 1400psi. The time histories of the temperature and the size of the droplet are recorded. The experimental vaporization histories are compared with existing analytical methods for the prediction of the droplet vaporization histories.

LIST OF SYMBOLS

A_P	projected plane area of droplet, ft^2
C_p	specific heat at constant pressure, $Btu/lb_m - {}^\circ R$
D	diameter of the droplet, ft
D_{AB}	binary diffusion coefficient, ft^2/hr
g	gravity constant, $(lb_m \cdot ft)/(lb_f \cdot sec^2)$
h	mean heat transfer coefficient, $Btu/ft^2 - hr - {}^\circ R$
ΔH_{LH}	latent heat of vaporization, Btu/lb_m
ΔH_{SH}	superheat of the vapor, Btu/lb_m
k	thermal conductivity, $Btu/ft - hr\ {}^\circ R$
k_{xm}	mass transfer coefficient, $lb_m/ft^2 - hr$
$\dot{m}''$	rate of mass transferred, $lb_m/ft^2 - hr$
P_c	critical pressure, lb_f/in^2
$\dot{q}''_{rad}$	heat transfer to droplet by radiation, $Btu/ft^2 - hr$
$\dot{q}_{th}$	heat transfer to droplet through thermocouples, Btu/hr
$\dot{q}''_T$	total heat transfer, $Btu/ft^2 - hr$
$\dot{q}''_d$	heat transfer to liquid droplet, $Btu/ft^2 - hr$
r	radius of droplet, ft, microns
T_e	environmental gas temperature, $^\circ R$
T_c	critical temperature, $^\circ R$
T_f	film temperature, $^\circ R$
T_d	droplet temperature, $^\circ R$
X_A	mole fraction of species A, dimensionless
σ	Boltzmann's constant, $Btu/ft^2 - {}^\circ R^4 - hr$
ρ	density, lb_m/ft^3

ρ_m mixture density, lb_m/ft^3

μ_m mixture viscosity, $lb_m/ft - hr$

θ_{AB} correction factor for high mass transfer rates, dimensionless

τ time, sec, hr

Subscripts

e_{ff} effective

f physical property evaluated at the film temperature

m physical property of the mixture

Superscripts

(') per ft

(") per ft^2

(˙) per sec

Dimensionless Groups

Nu Nusselt Number $\frac{hD}{k}$

Pr Prandtl Number $\frac{\mu C_p}{k}$

Nu_m Nusselt Number for mass transfer or the Sherwood Number $\frac{k_{xm} D}{\rho_{m_f} D_{AB_f}}$

Gr Grashof Number $\frac{D^3 \rho^2 g \beta \Delta T}{\mu^2}$

Gr_m Grashof Number for mass transfer $\frac{D^3 \rho_{m_f} g \xi (X_{A_s} - X_{A_\infty})}{\mu_m^2}$

Sc Schmidt Number $\frac{\mu_{m_f}}{\rho_{m_f} D_{AB_f}}$

LIQUID DROPLET EVAPORATION IN STAGNANT HIGH PRESSURE AND HIGH TEMPERATURE ENVIRONMENT

by T. P. Torda* and Robert Matlosz**

Illinois Institute of Technology
Chicago, Illinois

SUMMARY

The purpose of this research is the investigation of experimental vaporization histories for liquid droplets vaporizing in a subcritical, critical, and supercritical environment. The experimental research is concerned with a single droplet, suspended from a fine wire thermocouple, evaporating in a quiescent environment whose temperature and pressure approach, are equal to, or exceed the critical temperature and pressure of the vaporizing fuel droplet. The time histories of the droplet temperature and of the droplet size are recorded. The experimental radius-time histories are compared with existing analytical methods for the prediction of the droplet radius-time histories.

Experimental temperature-time and radius-time histories have been obtained for n-Pentane drops vaporizing in a nitrogen gas environment. The average initial diameter of the n-Pentane drops was 1828μ. The gas environment temperature was constant at 850°R for all experimental runs and the gas environment pressure was varied from 200psi to 1400psi.

A quasi-steady vaporization theory was used to calculate theoretical radius-time histories. The theoretical and experimental radius-time histories were compared and there was no correlation between the experimental results and the analysis. In an effort to explain the discrepancy, an energy balance was made on the vaporizing drop to determine the effects of radiation and of heat conduction through the thermocouple on the vaporizing drop. (The quasi-steady vaporization model does not account for the effects of radiation and of heat conduction through the thermocouple on the vaporizing droplet.) The results of the energy balance analysis indicated that the energy contributions from radiation and from the heat conduction through the thermocouple were small (approximately 2% to 3%) compared to the energy requirements for vaporization and superheat. Several conclusions were drawn from the energy balance analysis: 1) the quasi-steady vaporization theory is not valid for droplet evaporation at high temperatures and high pressures, and 2) a non-steady vaporization analysis using the equations of conservation of energy, momentum, mass, and species is required to solve this complex problem.

---

* IITRI Professor, Department of Mechanical and Aerospace Engineering
** Research Assistant, Graduate Student

INTRODUCTION

Systematic design and instability studies of liquid propellant rocket motors involve analytical modeling of the simultaneous interaction of complex thermodynamic and fluid dynamic processes. The important phenomena occurring in the rocket combustor include the dynamics of injection and stream breakup, oxidizer and propellant (droplet) vaporization, oxidizer and propellant vapor flow, mixing and dispersion, the chemical kinetics of combustion, and the gas dynamics of the combusted gas products.

Analytical models have been formulated for the design of liquid propellant rocket motors correlating the design parameters such as chamber pressures and temperatures, gas velocities and chamber geometries[1,2,3]. In these combustion models, propellant vaporization is assumed to be the rate controlling process. The justification of the assumption that the vaporization process is the rate controlling step based on the findings of Heidmann, Priem and Humphrey[4], Bittker[5], and Bittker and Brokaw[6] concerning the time and distance required for atomization, mixing, and chemical reactions. However, the validity of the vaporization rate controlled model at high chamber pressures is questionable, since there is lack of understanding concerning the vaporization phenomena in a supercritical gas environment (high chamber pressures and temperatures. Torda[7,8] indicated that liquid propellant droplets evaporating in a supercritical environment may remain in a transient heating state while vaporizing contrary to "normal" vaporization phenomena.* He concluded that a thorough investigation of the mechanism of droplet vaporization at elevated pressures and temperatures is a necessary requirement for a more valid rocket combustion model for design and instability studies. Further explanations of the phenomena of droplet vaporization under supercritical pressures have been either: 1) that the droplets are heated to an equilibrium wet-bulb temperature somewhat below the critical temperature, or 2) that the droplets undergo transient heating through the critical temperature[9]. Wieber[10] has shown that it is possible to predict analytically which of these two characteristic modes of behavior will take place under particular conditions depending upon how much of a droplet's mass is involved and how long the liquid-to-vapor transformation processes take. Combs[9] concluded from Wieber's analysis that if a droplet heats through its critical temperature it will no longer exhibit liquid properties but exist as dense pockets of supercritical fluid. The subsequent combustion rate would be controlled not by propellant vaporization but by the turbulent diffusion and mixing of the propellant vapors[11].

---

* The "normal" vaporization process is defined as droplet vaporization at a constant wet-bulb temperature. The aforementioned combustion models assume droplet vaporization at constant wet-bulb temperature.

Wieber's theoretical analysis of the calculated temperature histories of vaporizing droplets to the critical point is fundamental in the existing analytical modeling in liquid rocket engine combustion instability studies. Adjustments in the analytical model to account for the mode of droplet vaporization under the given chamber conditions are possible because Wieber's theoretical analysis predicts the mode of droplet vaporization under the given chamber conditions. However, Wieber indicates in his paper the apparent deficiencies in his theoretical development of droplet vaporization under supercritical environmental conditions. The foremost objection in the analysis is that the theory for droplet vaporization* has been developed at temperatures and pressures appreciably below the critical point of the fluid, whereas, a major fraction of the droplet's lifetime may be spent either in transient heating to its critical temperature while evaporating, or at some wet-bulb temperature below its critical temperature. Another objection in the analysis is the quasi-steady assumption of droplet vaporization,** but Wieber indicates that at the very worst, the analysis defines the upper limit of application of the theory which is the droplet heating to the critical temperature. Other investigators[16,17] disagree with this conclusion indicating that for environmental gas pressures greater than one-tenth the critical pressure of the vaporizing liquid, the vaporization (quasi-steady) theory is not valid.

It is apparent that experimental vaporization histories in supercritical environments are necessary either to verify existing theories or to formulate an improved theory. These experimental vaporization histories would necessarily include the mass, radius, and temperature-time variation for single droplets in varying high temperature and high pressure flow environments. Realizing the complexity of such an experimental apparatus required to obtain these time-dependent parameters, the more fundamental and less complex problem of droplet evaporation in a stagnant environment is thought to be a first step in the understanding of the supercritical vaporization phenomena encountered in rocket engines. Although the problem of droplet evaporation in a stagnant environment departs grossly from the real complex situation encountered in rocket combustors; the vaporization mechanism of a single stationary droplet, nevertheless, serves as a first indicator, or perhaps, as a reference in the behavior of propellants in one of the steps of the combustion process. Thus, the purpose of this research is the investigation of experimental vaporization histories for liquid droplets vaporizing in subcritical, critical, and supercritical environments.

---

* The theoretical analysis of the heat and mass transfer for a vaporizing spherical droplet is presented in References 12, 13, and 14. The theory involves the use of the empirical Nu=f(Re,Pr) correlation for spheres in forced heat convection obtained from experiment by Ranz and Marshall (Ref. 15). The analogy between heat and mass transfer is made; then, mass-time and temperature-time histories are predicted. Implicit in this analysis is the quasi-steady assumption of small time rate of change of drop size.

** This assumption is based on the supposition that the rate of change of droplet radius is small. However, for a vaporizing droplet whose temperature is near the critical temperature, the rate of change of droplet radius is not small.

The experimental research is concerned with a single droplet suspended from a thermocouple, evaporating in a quiescent environment whose temperature and pressure approach are equal to, or exceed the critical temperature and pressure of the vaporizing fuel droplet. The time histories of the temperature and size of the droplet are recorded. The experimental droplet vaporization histories are compared with existing analytical methods for the prediction of the droplet vaporization histories.

Experimental temperature-time and radius-time histories have been obtained for n-pentane drops vaporizing in a nitrogen gas environment. The average initial diameter of the n-pentane drops was 1828μ. The gas environment temperature was constant at 850°R for all experimental runs and the gas environment pressure was varied from 200psi to 1400psi.

A quasi-steady vaporization theory was used to calculate theoretical radius-time histories. The theoretical and experimental radius-time histories were compared and there was no correlation between the experimental results and the analysis. Since there was no agreement between the experimental results and the analysis, an energy balance was made on the vaporizing drop. The purpose of the energy balance was two-fold: 1) to determine the effects of radiation and of heat conduction through the thermocouple on the vaporizing drop, and 2) to calculate a design heat transfer coefficient which includes mass transfer. The results of the energy balance analysis indicated that the energy contributions from radiation and from the heat conduction through the thermocouple were small (approximately 2% to 3%) compared to the energy requirements for vaporization and superheat. Several conclusions were drawn from the analysis: 1) the analytical model (quasi-steady) is not valid for droplet vaporization at high temperatures and high pressures, and 2) a non-steady analysis using the energy, momentum, species, and global continuity equations is required to solve this complex problem.

DESCRIPTION OF THE EXPERIMENTAL APPARATUS AND TECHNIQUES

The apparatus for the experimental study consists of a test chamber pressurized with the appropriate gas (N_2, Air, Argon) and heated to a pre-selected equilibrium temperature in an electrical furnace. The liquid droplet is injected at a temperature which is lower than that of the chamber and is suspended from a fine wire thermocouple. The time history of the drop temperature is recorded using a Type RS 2-channel Dynograph Recorder and the time history of the drop size is recorded using a 16mm Bolex movie camera with close-up lenses. Photographs of the experimental apparatus and the explanation of the various equipment are shown in Figures 1 and 2. A schematic diagram of the experimental apparatus is shown in Figure 3.

Two test chambers are used in the experimental study. The low to intermediate pressure test chamber (a modified stainless steel sight flow indicator*) is used in droplet vaporization experiments with environmental gas conditions up to 600psi and 1000°R. The test chamber, shown in Figure 5, has a total volume (under experimental conditions) of 39.67 cubic inches. Three windows have been incorporated in the modification of this test chamber: one window is used for photography, the second window is used for lighting, and the third window is used for observation. The windows of the test chamber are 5/8" thick tempered Pyrex glass discs. The sealing gaskets for this test chamber are 1/8" thick teflon flat gaskets.

To permit droplet vaporization experiments at elevated pressures and temperatures beyond the limits of the intermediate pressure vessel, a high-pressure test chamber has been used in experiments with environmental gas conditions up to 1500psi and 1200°R. The high pressure test chamber is shown in Figure 4. The design specifications and the assembly drawings of the high pressure vessel are presented in Appendix I.

A water cooled droplet injector system was designed for both test chambers to enable successful droplet injection and suspension from a thermocouple at elevated temperatures and pressures. A typical droplet injector with the droplet support thermocouple and the local temperature thermocouple is shown in Figure 7. The technique of droplet injection into the pressurized test chamber was developed using three control valves. A schematic drawing of the arrangement of the droplet injection control valves is shown in Figure 8. A small pressure difference (25psi) is applied across the liquid supply tank and the test chamber. The liquid line control valve (A) is opened and the fluid flows into the injector. When the liquid emerges from

---

* A sight flow indicator is used in piping systems for visual indication of flow conditions. The indicator used in the experiment is a Model #8001 Brooksight Sight Flow Indicator from Brooks Instrument Co., Hatfield, Pennsylvania.

the injector tip, control valve (A) is closed. Valve (B) is opened and a momentary back flow of the liquid in the injector is caused by the pressure difference across valve (B) until the small volume between valve (B) and (C) is filled with the liquid. Valve (B) is closed and valve (C) is then opened and the liquid in the small volume is expelled to the air environment. When the control valves are manipulated in the above manner, several droplets or possibly a single droplet can be injected into the pressurized test chamber.

The drop size time history is recorded using the 16mm Bolex movie camera with an 85mm focal length lense and a +3 diopter lense. The physical area covered at minimum focusing distance is 23mm x 18mm.

Experimental Results

Experimental vaporization histories have been obtained for n-pentane droplets evaporating in a nitrogen gas environment at 850°R and a range of pressures from 200psi to 1400psi. The temperature time histories are presented in Figure 9 and the experimental radius time histories are shown in Figure 10. The average initial drop diameter was 1828μ and the average initial droplet temperature was 576°R.

The experimental radius time histories have been obtained by the following technique. Using a 16mm movie projector, the droplet images on the film are projected onto a mat white screen. This screen permits the reproduction of very sharp images. The projected plane area of the droplet, A_p, is measured with a planimeter and is equated to a circular area with an effective radius r_{eff}. Thus

$$A_p = \pi r_{eff}^2$$

or, solving for r_{eff}

$$r_{eff} = \sqrt{\frac{A_p}{\pi}}$$

The r_{eff} was chosen as the characteristic radius dimension because the droplet shape was somewhat spherical and axially symmetric. Axial symmetry of the vaporizing droplet was verified by photographing the droplet at right angles and comparing the measured plane areas. However, valid drop size data using this technique could only be obtained to approximately 70% of the initial droplet effective radius remaining. Beyond this point the droplet was deformed due to the presence of the thermocouple. The drop size time relationship is known through synchronization of the camera and recorder, and an effective radius time history was then obtained.

Table I is a listing of the experimental runs for n-pentane drops vaporizing in N_2 gas at 850°R and a range of pressures from 200psi to 1400psi. These experimental runs were selected on the basis of initial drop size, initial temperature and lead time.* Selection of experimental data is important because, due to variation in injection techniques (manual operation), initial drop size and amount of fluid injected into the chamber can vary. Such variation influences experimental results. Five representative experimental runs were selected from the list in Table I which have the smallest deviation from the mean in initial radius and initial temperature.

---

* Lead time is the time from initial liquid injection to the time when a droplet is formed on the thermocouple. Thus the lead time is a crude measure of the amount of liquid injected into the chamber prior to droplet formation.

ANALYSIS

A quasi-steady vaporization theory for droplets evaporating in a quiescent environment with natural convection was used to calculate theoretical radius time histories. The detailed development of the quasi-steady vaporization theory and the computational procedure is presented in Appendix II. The calculated and experimental radius time histories for the 200psi and the 1400psi runs are compared and shown in Figure 13. Since there is no agreement between the theoretical analysis and the experimental results an energy balance was made on the vaporizing drop. The purpose of the energy balance was two-fold: 1) to determine the effects of radiation and of heat conduction through the thermocouple on the vaporizing drop, and 2) to calculate a design heat transfer coefficient which includes mass transfer.

The first objective of the energy balance analysis indicates whether or not the quasi-steady vaporization model with natural convection is applicable, since the vaporization model does not account for droplet heating due to radiation and heat conduction through the thermocouple.* If the energy contributions from radiation and/or heat conduction through the thermocouple are negligible compared to the energy requirements for latent heat of vaporization and superheat, then the discrepancy between the calculated and experimental radius time histories cannot be explained in terms of the effects of radiation and of heat conduction through the thermocouple on the evaporation of the droplet.

The second objective of the energy balance analysis is meaningful only if the effects of radiation and of heat conduction through the thermocouple are negligible compared to the energy requirements for latent heat of vaporization and superheat. Then the calculated heat transfer coefficients can be used as design heat transfer coefficients for evaporating droplets.

The equation of conservation of energy for the vaporizing droplet is written as follows

ENERGY ADDED = ENERGY REQUIRED FOR VAPORIZATION + ENERGY STORED (1)

The energy added (from all sources) to the vaporizing droplet is

$$q_T = h(T_e - T_d)4\pi r^2 d\tau + \sigma(T_e^4 - T_d^4)4\pi r^2 d\tau + q_{th} d\tau$$

energy addition from environment	energy addition by radiation	energy addition through thermocouple

---

* The energy contributions for droplet evaporation from radiation and heat conduction through the thermocouple affect the experimental radius time histories of the vaporizing droplet. These effects are included in the experimental radius time histories, whereas, the radiation and heat conduction effects on the vaporizing droplet are not included in the analytical model.

The energy required for vaporization (including superheat of the vapors) is

$$4\pi r^2 \rho (\Delta H_{LH} + \Delta H_{SH}) dr$$

The energy stored in the liquid drop is

$$\rho C_p \frac{4}{3} \pi r^3 dT$$

Substituting the above expression into equation (1), the resulting energy balance equation is

$$h(T_e - T_d) + \sigma(T_e^4 - T_d^4) + \frac{q_{th}}{4\pi r^2} = \rho(\Delta H_{LH} + \Delta H_{SH})\frac{dr}{d\tau} + \frac{rC_p\rho}{3}\frac{dT}{d\tau} \qquad (2)$$

environment — radiation — thermocouple — vaporization — storage

The various energy contributions are identified below equation (2). Black body radiant energy transfer was assumed in calculating the energy contribution to the vaporizing droplet due to radiation. The heat conduction through the thermocouple, q_{th}, was calculated using the theory of heat transfer from fins.* The quantities $\frac{dr}{d\tau}$ and $\frac{dT}{d\tau}$ were obtained from the experimental radius time and temperature time histories respectively. The heat transfer coefficient, h, was calculated using equation (2), and the various energy contributions were also calculated using the following equations

$$\dot{q}''_{rad} = \sigma(T_e^4 - T_d^4)$$

$$\dot{q}''_T = h(T_e - T_d) + \dot{q}''_{rad} + \dot{q}_{th}/4\pi r^2$$

$$\dot{q}''_d = \dot{q}''_T - H_{SH}\frac{dr}{d\tau} = \dot{q}''_T - \dot{q}''_{SH}$$

$$\%\, q_{th} = \frac{\dot{q}''_{th}}{\dot{q}''_d} 100\ \% \qquad \%\, q_{rad} = \frac{\dot{q}''_{rad}}{\dot{q}''_d} 100\ \%$$

---

* The heat transfer to the liquid droplet through the thermocouple was calculated assuming: 1) that the liquid droplet is a heat sink at temperature T_d, and 2) that the thermocouple wires extending from the liquid droplet are infinitely long pins in an environment at temperature T_e.

The results of the energy balance analysis are shown in Table II and it may be seen that the energy contributions from radiation and from heat conduction through the thermocouple are small compared to the energy requirements for vaporization and superheat. Thus, the discrepancy between the calculated and experimental radius time histories cannot be explained in terms of the effects of radiation and of heat conduction through the thermocouple on the evaporation of the droplet. Several conclusions are drawn from the energy balance analysis: 1) the quasi-steady vaporization theory is not valid for droplet evaporation at high temperatures and high pressures (supercritical environmental conditions), and 2) a non-steady vaporization theory using the energy, momentum, species, and global continuity is required to solve this complex problem.

SUMMARY AND RECOMMENDATIONS

Several useful objectives have been accomplished in the experimental research:

1) Reproducible temperature time and radius time histories for droplets vaporizing in a quiescent high pressure and high temperature environment have been obtained from the experiment, and at the very least, these results are the first step in the understanding of the supercritical vaporization phenomena.

2) A quasi-steady vaporization model has been shown to be not valid in predicting radius time histories for droplet evaporation at high pressures and high temperatures.

3) From the energy balance, a realistic design heat transfer coefficient, h, which includes mass transfer, was calculated using the experimental radius time and temperature time histories of the vaporizing drop.

Since the experimental radius time and temperature time histories for the vaporizing droplet do not agree with the recommended quasi-steady (heat-mass transfer analogy) vaporization theory, it is imperative to carry out a non-steady droplet vaporization analysis beginning with the equations of conservation of energy, momentum, mass, and species. In addition to the development of a non-steady vaporization analysis, experimental vaporization histories should be obtained for other liquid propellants.

APPENDIX I

DESIGN SPECIFICATIONS OF THE HIGH PRESSURE TEST CHAMBER

The stainless steel high pressure test chamber was fabricated in the machine shop of the Mechanical and Aerospace Department at Illinois Institute of Technology. The high pressure test chamber is shown in Figure 4. The assembly drawing of the high pressure test chamber is shown in Figure 14.

The material of the test chamber, type 321 stainless steel, was chosen because of its high resistance to corrosive propellants.

The three windows of the pressure vessel are ground and polished, optical quality, quartz glass. The main (window) flanges were designed to permit an increased positive seal with an increase in pressure (self sealing system). Metal V-seals* are used both in the window-to-flange sealing surfaces (item F of the assembly drawing) and in the main flange-to-block sealing surfaces (item E of the assembly drawing). The components of the flange assembly for the high pressure vessel are shown in Figure 6.

The total internal volume of the high pressure vessel is 64.1 cubic inches.

The high pressure test chamber was hydrostatically tested to 2800psi at room temperature. The test chamber has been used in experiments with environmental gas conditions up to 1500psi and 1200°R.

---

* Parker Seal Company, Culver City, California

APPENDIX II

THE QUASI-STEADY VAPORIZATION THEORY FOR DROPLETS EVAPORATING IN A QUIESCENT ENVIRONMENT WITH NATURAL CONVECTION

The Quasi-Steady Vaporization Theory for droplets evaporating in a quiescent environment with natural convection involves the use of the empirical $Nu = f(Gr,Pr)$ correlation for spheres in free heat convection. The analogy between heat and mass transfer is made to calculate mass transfer rates from the corresponding empirical heat transfer correlation. Such an analogy permits the derivation of mass transfer correlations from heat transfer correlation for spheres in natural convection for equivalent boundary conditions by merely substituting the Nusselt Number for mass transfer for the Nusselt Number for heat transfer, the Grashof Number for mass transfer for the Grashof Number for heat transfer, and the Schmidt Number for the Prandtl Number. The assumptions in order to obtain this analogy are: 1) constant physical properties, 2) small rate of mass transfer, and 3) isothermal mass transfer.

The constant physical property restriction can be handled by defining a film temperature $T_f = \frac{T_d + T_e}{2}$. The physical properties are assumed constant and evaluated at the temperature T_f.

The second restriction of low mass transfer rates is removed by inserting a correction factor θ_{AB} for the mass transfer coefficient k_{xm} dependence on the mass transfer rate.

The isothermal mass transfer restriction is the most serious of the three restrictions on the analogy between heat and mass transfer. The experimental results indicate that the vaporization process is definitely non-isothermal. However, the mass transfer rates were calculated for an isothermal mass transfer problem by varying the operating temperature level according to the experimental temperature time history.

For the case of droplet evaporation in a stagnant environment, the corresponding heat transfer correlation is the empirical relation for free convection[15]

$$\frac{hD}{k} = 2.0 + 0.6 \cdot \left[\frac{D^3 \rho^2 g \beta \Delta T}{\mu^2}\right]^{\frac{1}{4}} \cdot \left[\frac{C_p \mu}{k}\right]^{\frac{1}{3}} \tag{1}$$

Assuming the analogy for heat and mass transfer and making the appropriate dimensionless numbers substitution, the resulting mass transfer correlation is

$$\frac{k_{xm} D}{\rho_{mf} D_{AB_f}} = 2.0 + 0.6 \cdot \left[\frac{D^3 \rho^2_{mf} \xi g (X_{A_S} - X_{A_\infty})}{\mu^2_{mf}}\right]^{\frac{1}{4}} \cdot \left[\frac{\mu_{mf}}{\rho_{mf} D_{AB_f}}\right]^{\frac{1}{3}} \tag{2}$$

where

$$\xi = \frac{1}{\rho_{mf}} \left(\frac{\partial \rho_m}{\partial x_A}\right)_{T,P} \qquad \beta = \frac{1}{\rho}\left(\frac{\partial \rho}{\partial T}\right)_P$$

and the other symbols are defined in the List of Symbols. The subscript (f) indicates that all physical properties are evaluated at the film temperature T_f.

The diffusion coefficient, D_{AB}, was evaluated using the modified Hirschfelder, Bird, and Spotz method,[18] so that the expression for the diffusion coefficient is

$$D_{AB} = \frac{BT^{\frac{3}{2}}\left[\frac{M_A+M_B}{M_AM_B}\right]^{\frac{1}{2}}}{Pr_{AB}^2 W^{(1)}_{(1-\Delta)}} \tag{3}$$

where

$$B = 10.7 - 2.46\left[\frac{M_A+M_B}{M_AM_B}\right]^{\frac{1}{2}} \cdot 10^{-4}$$

$$r_{AB} = \frac{r_A+r_B}{2}$$

r_A, r_B collision radii for component A and B, respectively

$W^{(1)}$ collision integral as a function of $\frac{\sigma T}{\varepsilon}$

ε energy of attraction

σ Boltzmann's constant

Although little experimental data is available on the pressure effects on D_{AB}, Campbell[19] indicates that the H.B.S. equation, presented in Reid and Sherwood[20] is valid (to within approximately 10%) up to 100 atmospheres. Figure 11 shows the diffusion coefficient, D_{AB}, as a function of the temperature for n-Pentane-Nitrogen gas system.

The expression for ξ was calculated using the following equations

$$P_T = P_A + P_B \tag{4}$$

where

P_T is the total pressure

P_A is the partial pressure of component A

P_B is the partial pressure of component B

$$X_A = \frac{\frac{\rho_A}{M_A}}{\frac{\rho_A}{M_A} + \frac{\rho_B}{M_B}} \tag{5}$$

$$\rho_m = \rho_A + \rho_B \tag{6}$$

$$1 = X_A + X_B \tag{7}$$

The Van der Waals equation of state

$$\left(P + \frac{a}{V^2}\right) \cdot (V - b) = RT \tag{8}$$

was used in the analysis because the equation holds fairly well in the vapor region and near and above the critical point[21].

Using equations (4) through (8) the expression for ξ was calculated by first choosing the total pressure and temperature. Then, the density of n-Pentane vapor (species A) was chosen and P_A was calculated from the Van der Waals equation. With P_A calculated, P_B was obtained from the pressure relationship (Equation (4)). Using the Van der Waals equation of state for component B, ρ_B was calculated knowing P_B. The mixture density was then computed from equation (6). The mole fraction of component A, X_A, was calculated from equation (5). The process was then repeated for several data points until a relationship between ρ_m and X_A was plotted. The relationship was linear and hence

$$\rho_m \cdot \xi = \left(\frac{\partial \rho_m}{\partial X_A}\right)_{T,P} = \text{constant}$$

The total pressure and the temperature were varied such that a relationship for $\rho_m \cdot \xi$ as a function of pressure and temperature was obtained. The resulting is shown in Figure 12.

The gas film mixture viscosity μ_m was calculated using the expression[22]

$$\mu_m = \frac{\mu_A}{1 + \frac{1.385\mu_A X_B}{D_{AB}\rho_A X_A}} + \frac{\mu_B}{1 + \frac{1.385\mu_B X_A}{D_{AB}\rho_B X_B}} \qquad (9)$$

where

μ_A, μ_B are the viscosities of the pure components A and B at the temperature of the mixture.

ρ_A, ρ_B are the densities of the pure components A and B at the temperature and total pressure.

X_A, X_B are the mole fractions of the components A and B of the mixture in the film.

Specifying the initial droplet diameter and the droplet temperature from the experimental data, the mass transfer coefficient k_{xm} was calculated from equation (2). The rate of mass transfer was calculated by

$$\dot{m}'' = k_{xm} \cdot B \qquad (10)$$

where

k_{xm} is the mass transfer coefficient (or conductance).

$B = \frac{X_{A_s} - X_{A_\infty}}{1 - X_{A_s}}$ is the driving potential for mass transfer.

A correction factor θ_{AB} for the k_{xm} dependence on the mass transfer rate (from film theory) is[23,24]

$$\theta_{AB} = \frac{\ln(1+B)}{B} \qquad (11)$$

The resulting equation for calculating the mass transfer rate is

$$\dot{m}'' = k_{x\dot{m}}\theta_{AB}B = k_{x\dot{m}}\ln(1+B) \qquad (12)$$

Knowing $\dot{m}''$ from equation (12), a volume change was calculated from

$$\Delta V = \frac{\dot{m}'' A_S \Delta\tau}{\rho_L} \qquad (13)$$

where

A_S is the mean surface area of the droplet.

$\Delta\tau$ is a small increment of time.

ρ_L is the liquid density of the droplet at the temperature obtained from the experimental temperature-time history.

From the volume change a new radius at $\Delta\tau$ time later was calculated and the calculations were repeated to obtain the radius-time history. Figure 13 shows the calculated and the experimental radius-time histories for the 200psi and 1400psi runs.

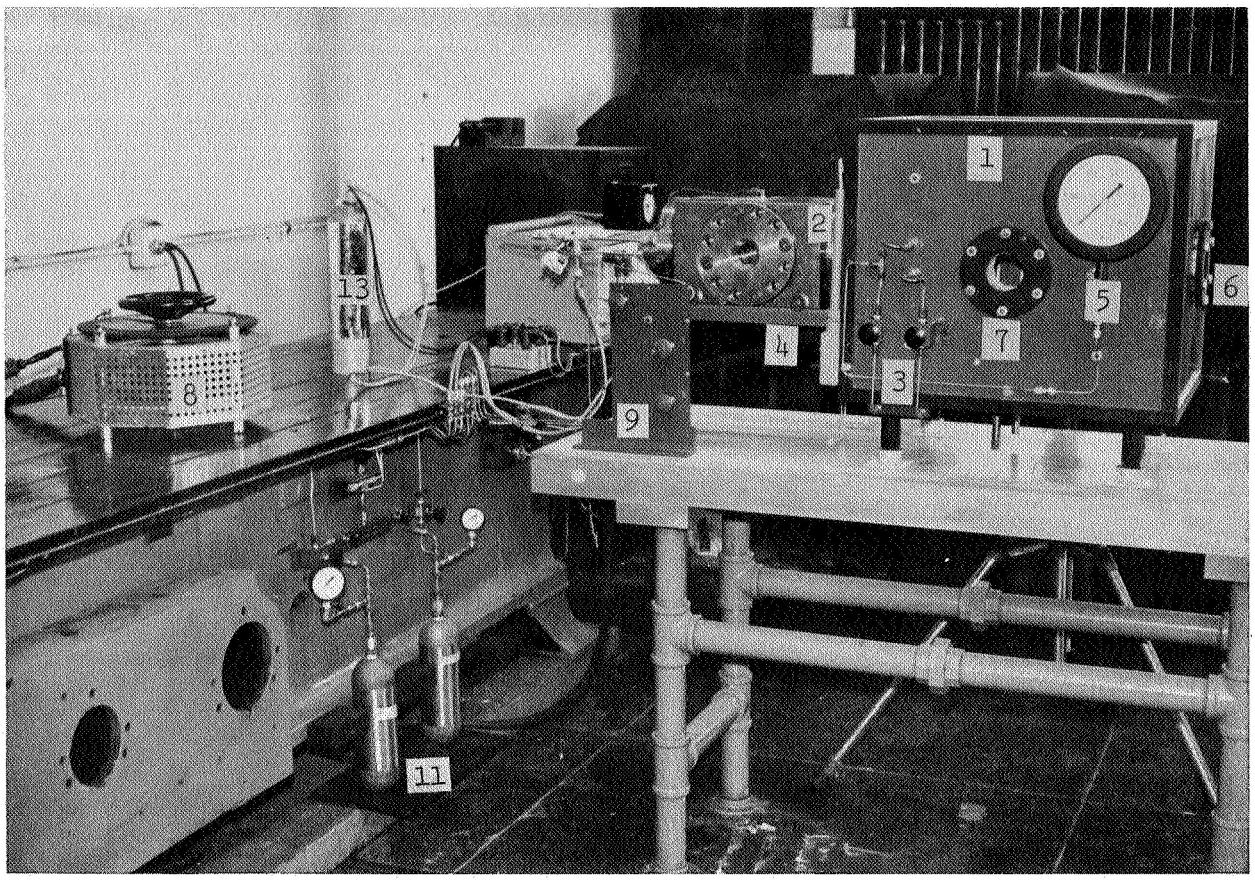

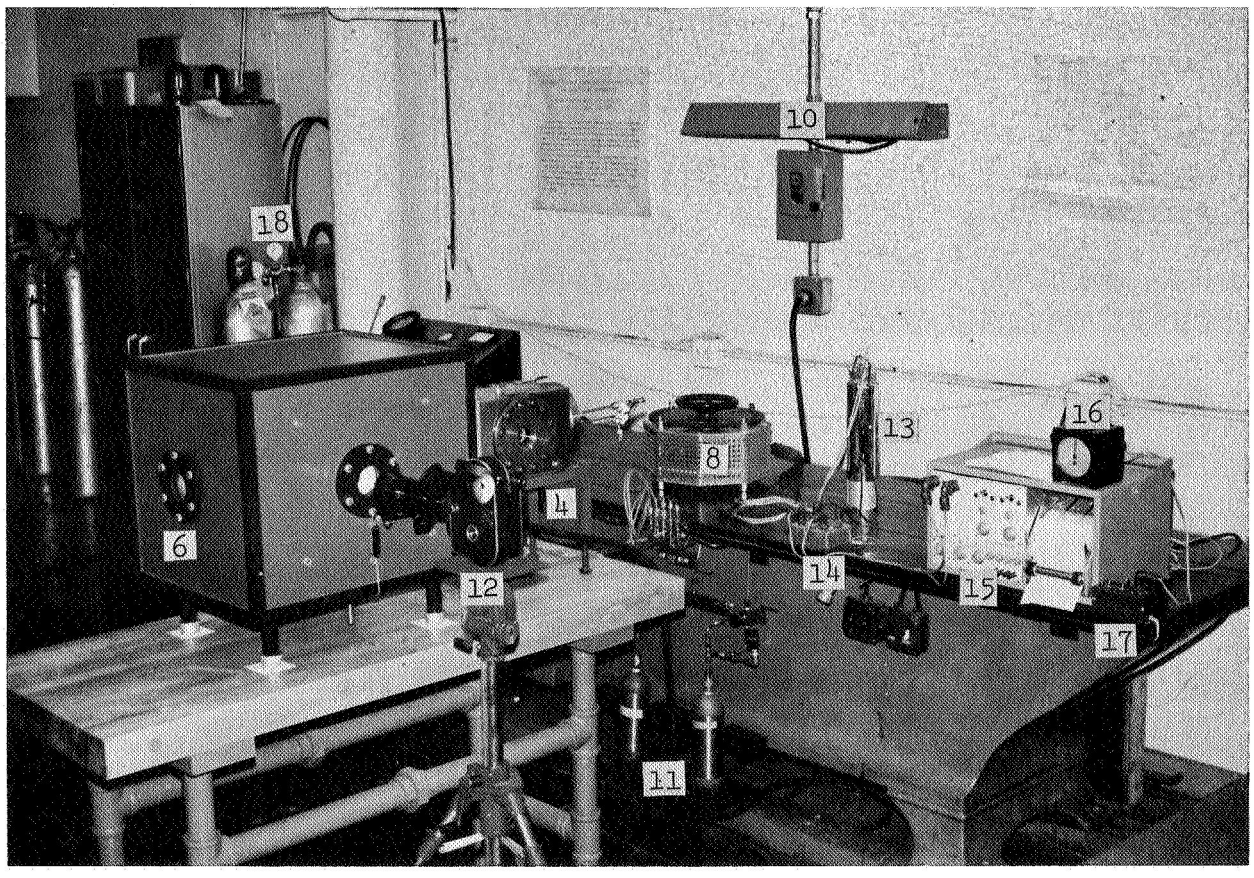

Figure 1. Photographs of the Experimental Apparatus

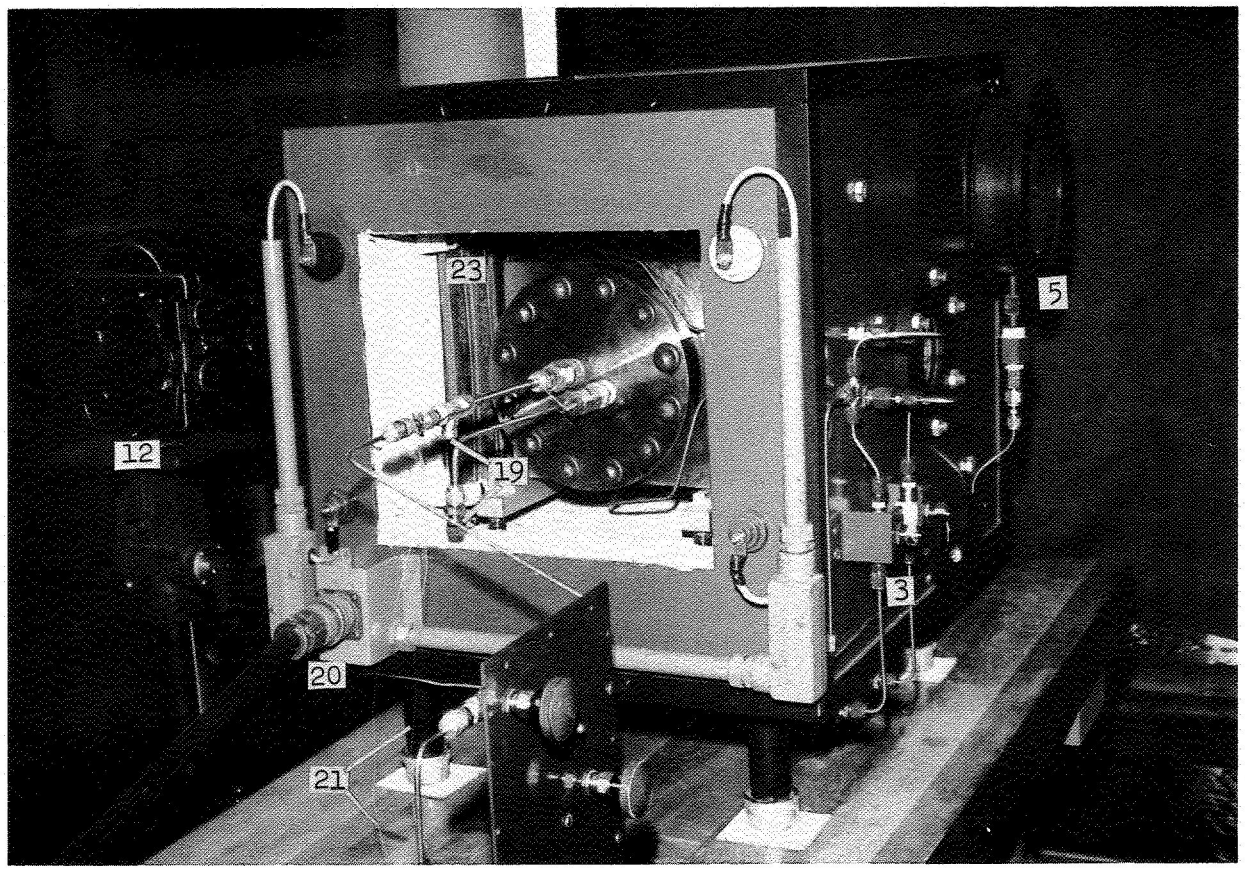

Figure 2. Photograph of the High Pressure Vessel Inside the Electrical Furnace with Furnace Doors Removed

Explanation of Figures 1 and 2

1. Electrical furnace 5.5 kw power capacity 1700°R maximum temperature.
2. Stainless steel high pressure vessel.
3. Control valves for environmental gas isolation and environmental gas purging.
4. Rail stand to permit easy handling of test chamber.
5. Environmental gas pressure gauge.
6. Infrared filter window for lighting.
7. Visual observation window.
8. Powerstat for oven temperature control.
9. Droplet injection control valves.
10. 240 volt, 3 phase power source for electric furnace.
11. Liquid propellant storage tanks.
12. Bolex 16mm camera with variable focal length lens and 3 diopter for close-up photography.
13. Ice (cold junction) bath for thermocouple.
14. Electrical switch for interrupting signal input to recorder.
15. Two channel Dynograph Type RS Recorder.
16. Electric timer.
17. Electrical switch for synchronizing the camera film and recorder output data.
18. Environmental gas supply tanks.
19. Water input and return tubes for coolant.
20. Electrical power connection for the furnace.
21. Stainless steel sheathed thermocouple leads.
22. Electrical strip heaters.

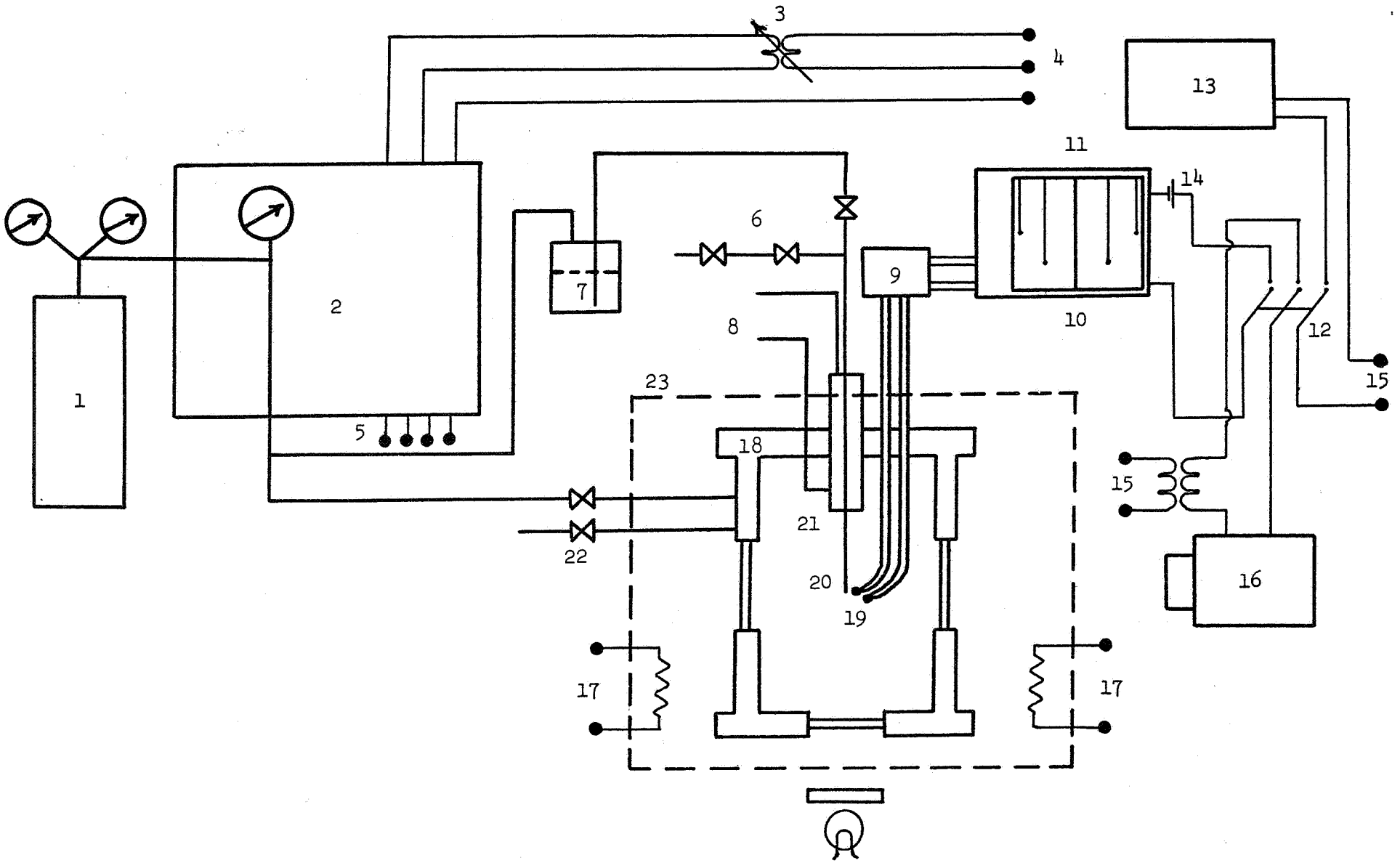

Figure 3. Schematic diagram of the experimental apparatus.

Explanation of Figure 3

1. Environmental gas supply tank.
2. Control panel.
3. Powerstat for oven temperature control.
4. 240 volt, 3 phase power source for electrical furnace.
5. Four electrical power terminals wired to the resistance heaters of the oven.
6. Droplet injection control valves.
7. Liquid propellant storage tank.
8. Water input and return tubes for coolant.
9. Ice (cold junction) bath for thermocouples.
10. Two channel Dynograph Type RS Recorder.
11. Event markers.
12. Electrical switch for synchronizing the camera film and recorder output data.
13. Electric timer.
14. 6 volt D.C. source used to trip event marker when electric switch is closed.
15. 120 volt, single phase A.C. source.
16. Bolex 16mm camera and motor drive.
17. Electrical resistance heaters.
18. Pressure vessel.
19. Thermocouples.
20. Injector.
21. Injector cooling jacket to prevent the liquid propellant from vaporizing before injection.
22. Control valves for environmental gas isolation and environmental gas purging.
23. Oven boundary.

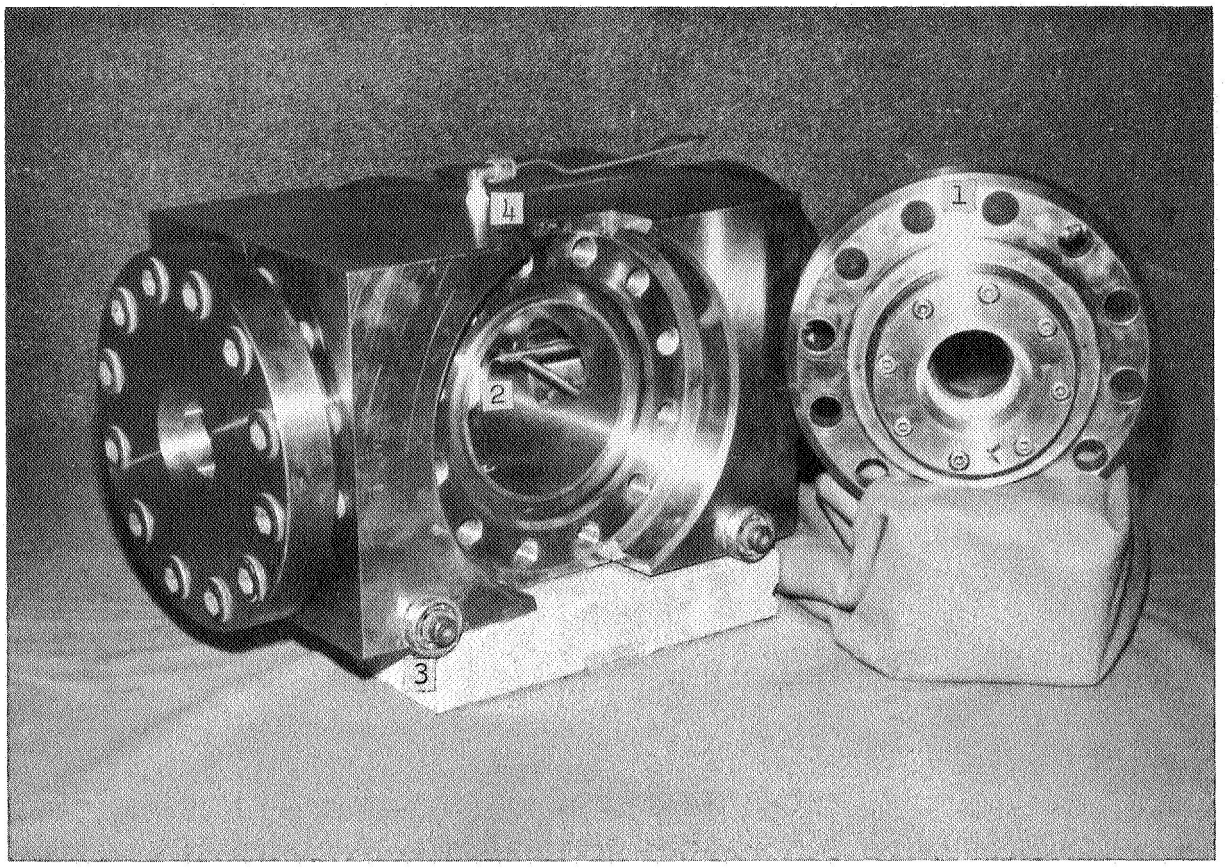

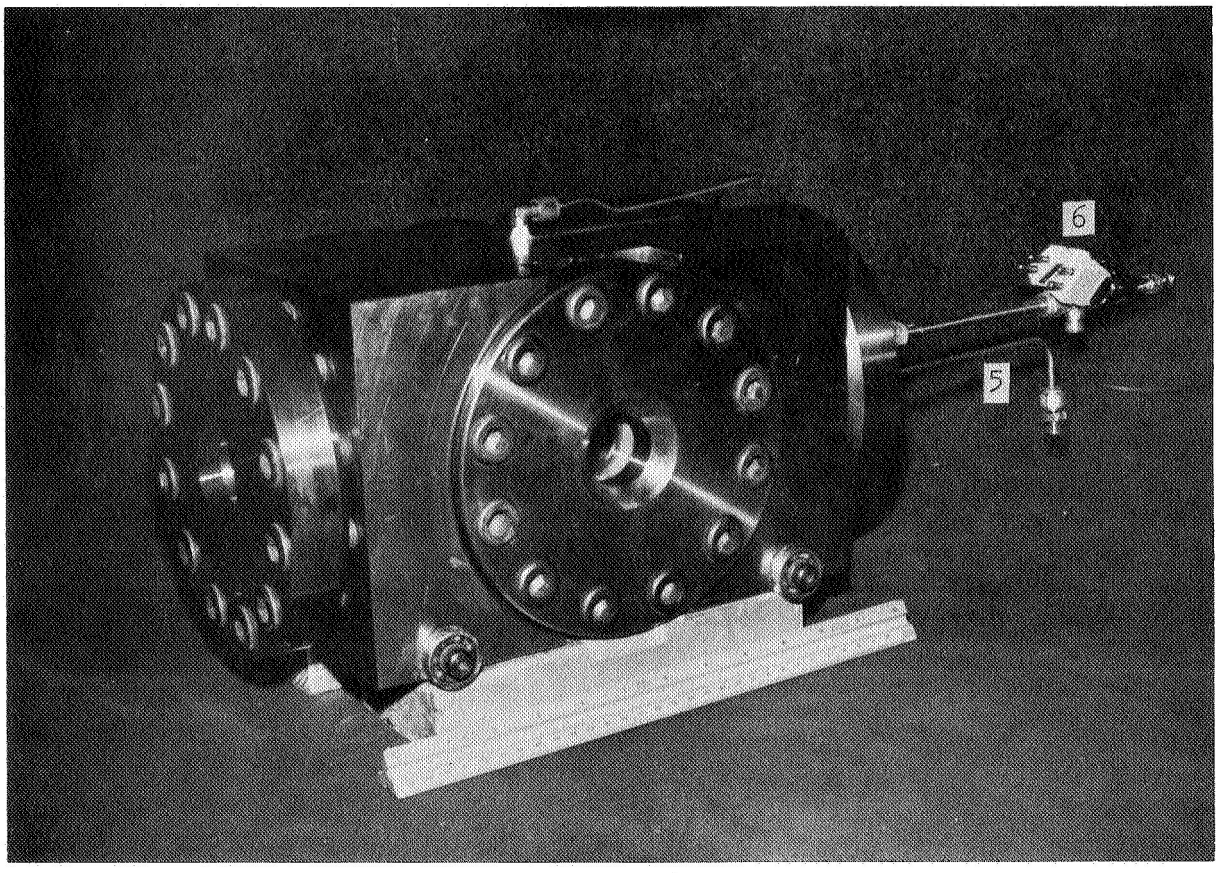

Figure 4. Photographs of the High Pressure Vessel

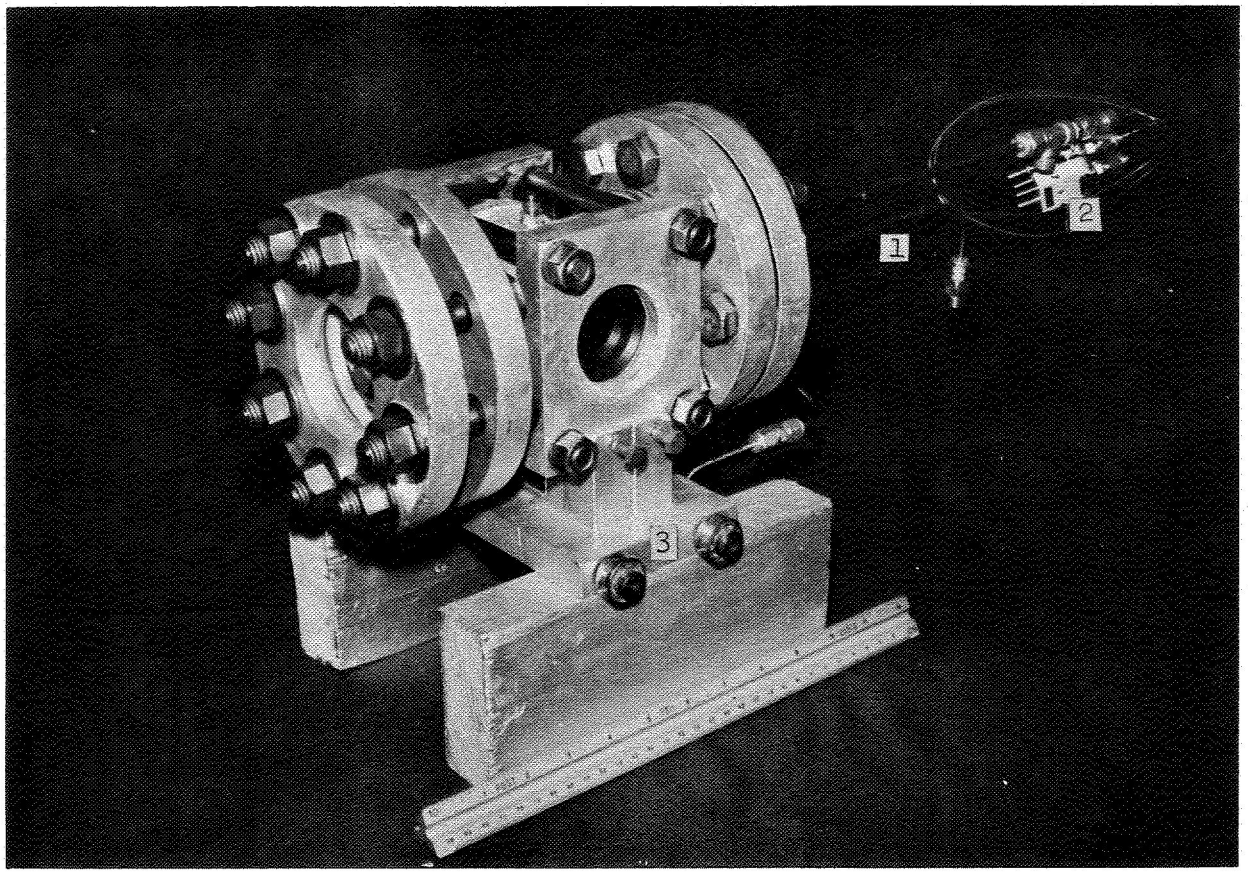

Figure 5. Photograph of the Low - Intermediate Pressure Vessel

Explanation of Figure 4

1. Typical Flange Assembly - Three required.
2. Injector and Injector-Cooling System.
3. Roller Bearings for easy handling of the pressure vessel.
4. Environmental gas supply tubing.
5. Injector Cooling Jacket.
6. Thermocouple Jacks.

Explanation of Figure 5

1. Injector Cooling Jacket.
2. Thermocouple Jacks.
3. Pressure Vessel Stand and Roller Bearings.

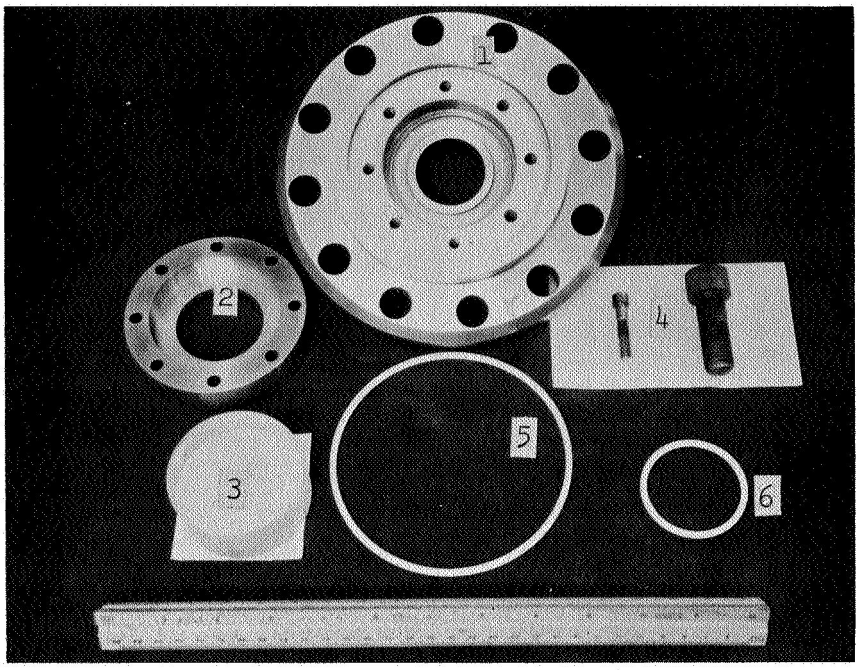

Figure 6. The Components of the Flange Assembly for the High Pressure Vessel

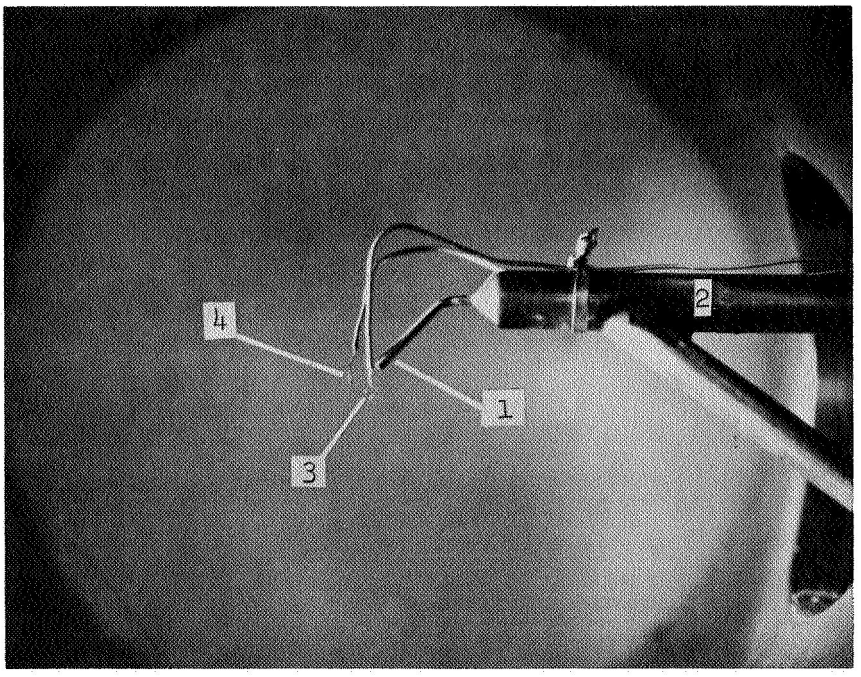

Figure 7. Typical Arrangement for the Injector, Injector Cooling Jacket, and Thermocouples

Explanation of Figure 6

1. Main flange.
2. Auxiliary flange.
3. Quartz Window Glass.
4. Alloy cover bolts.
5. V-Seal for main flange.
6. V-Seal for auxiliary flange.

Explanation of Figure 7

1. Injector tip.
2. Cooling jacket for injector line.
3. Droplet support thermocouple.
4. Local temperature thermocouple.

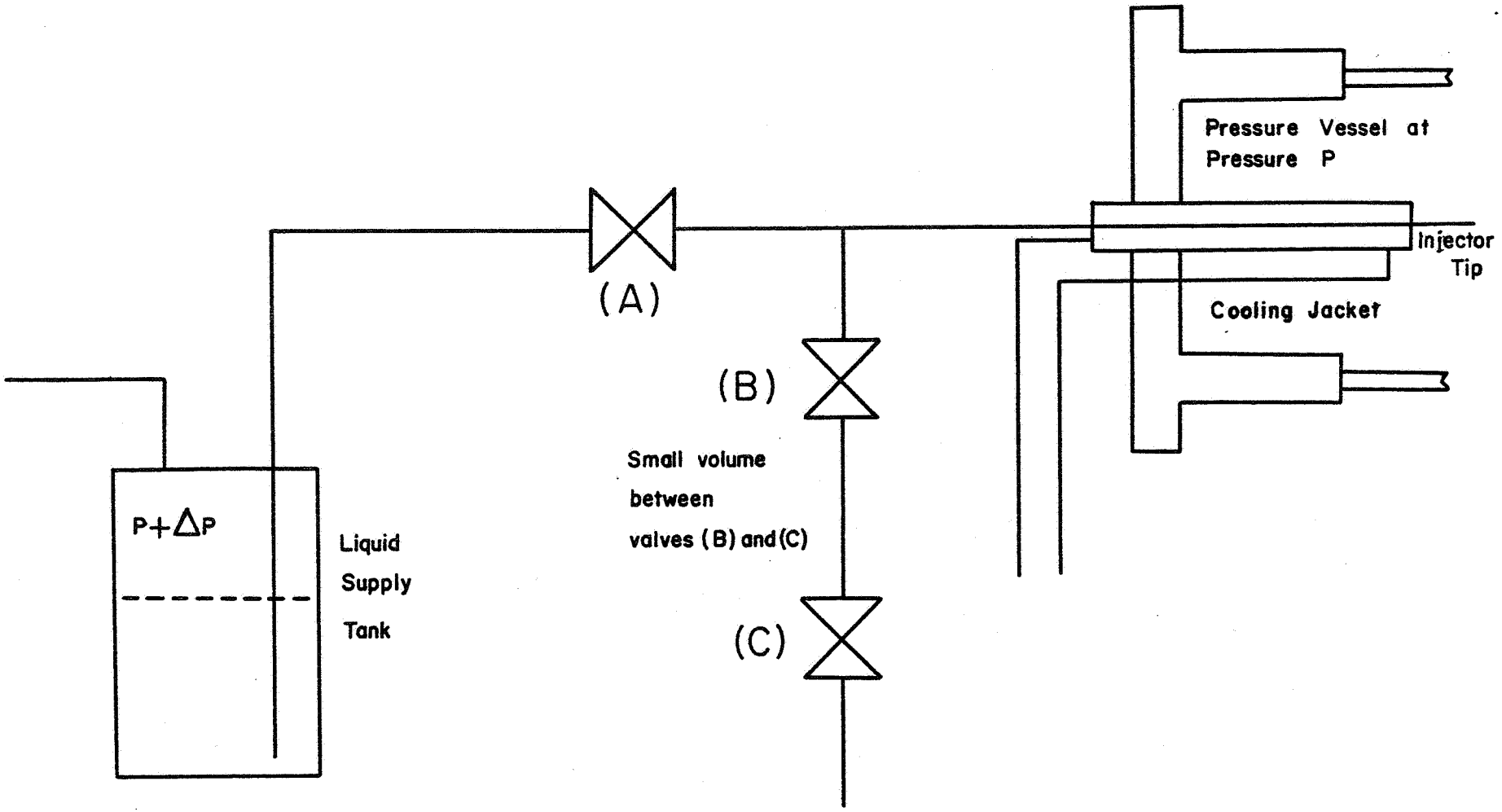

Figure 8. Schematic diagram of the droplet injection control valves.

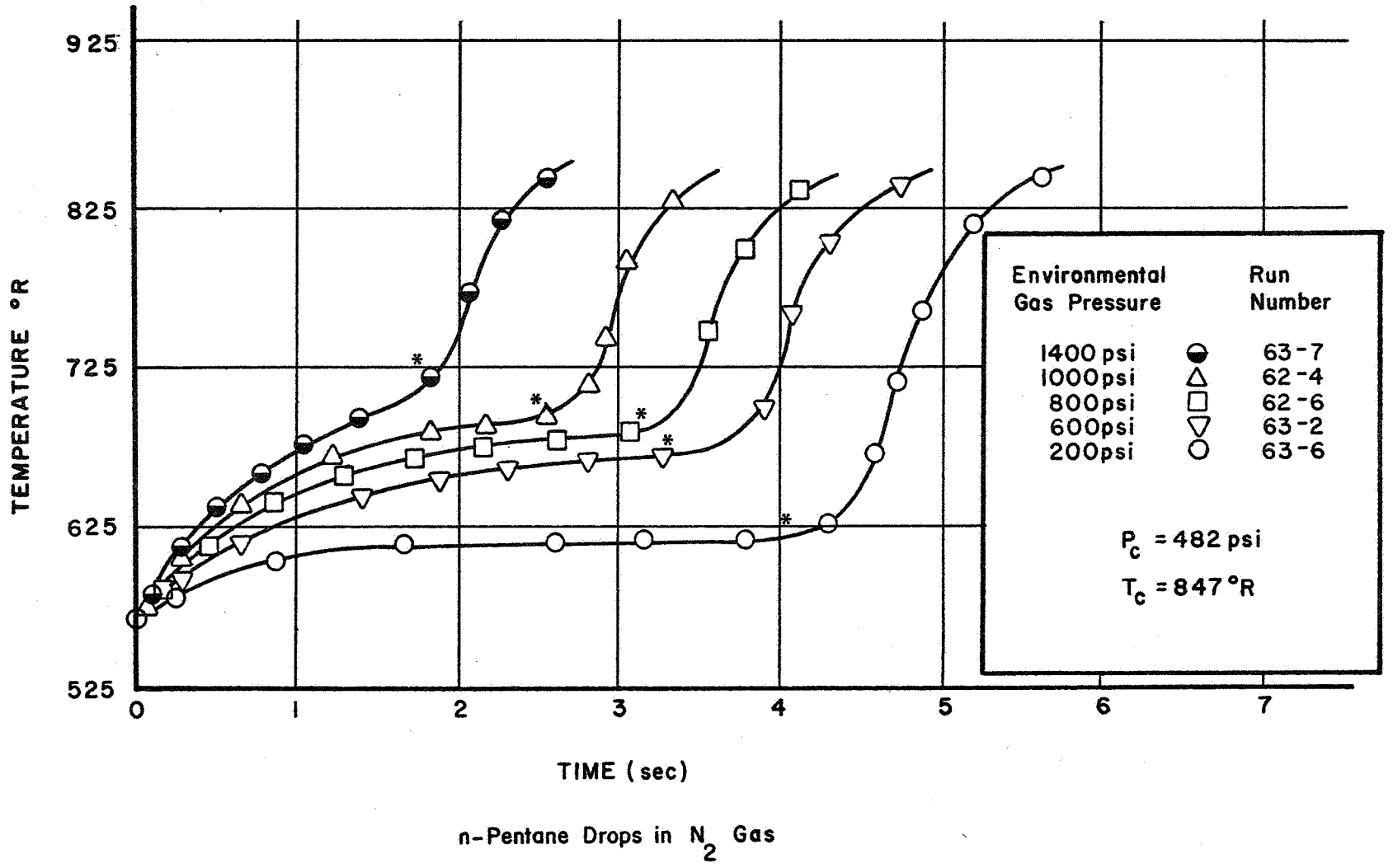

Figure 9. Experimental Temperature-time Histories at Different Environmental Gas Pressures. Environmental Gas Temperature 850 °R. Asterisk (*) indicates the observed time for droplet vaporization.

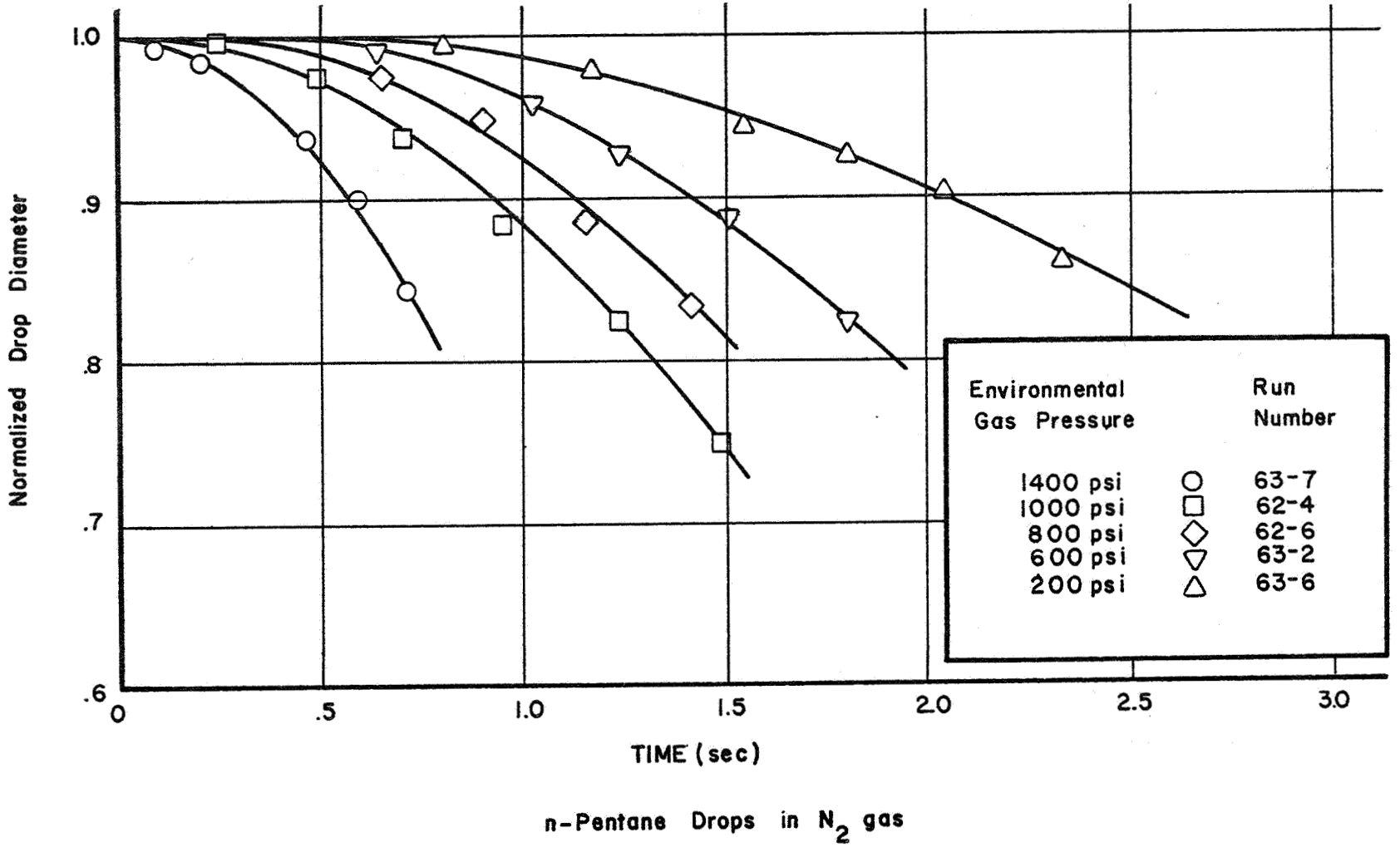

Figure 10. Experimental Radius-time Histories at different Gas Pressures. Environmental Gas Temperature 850° R.

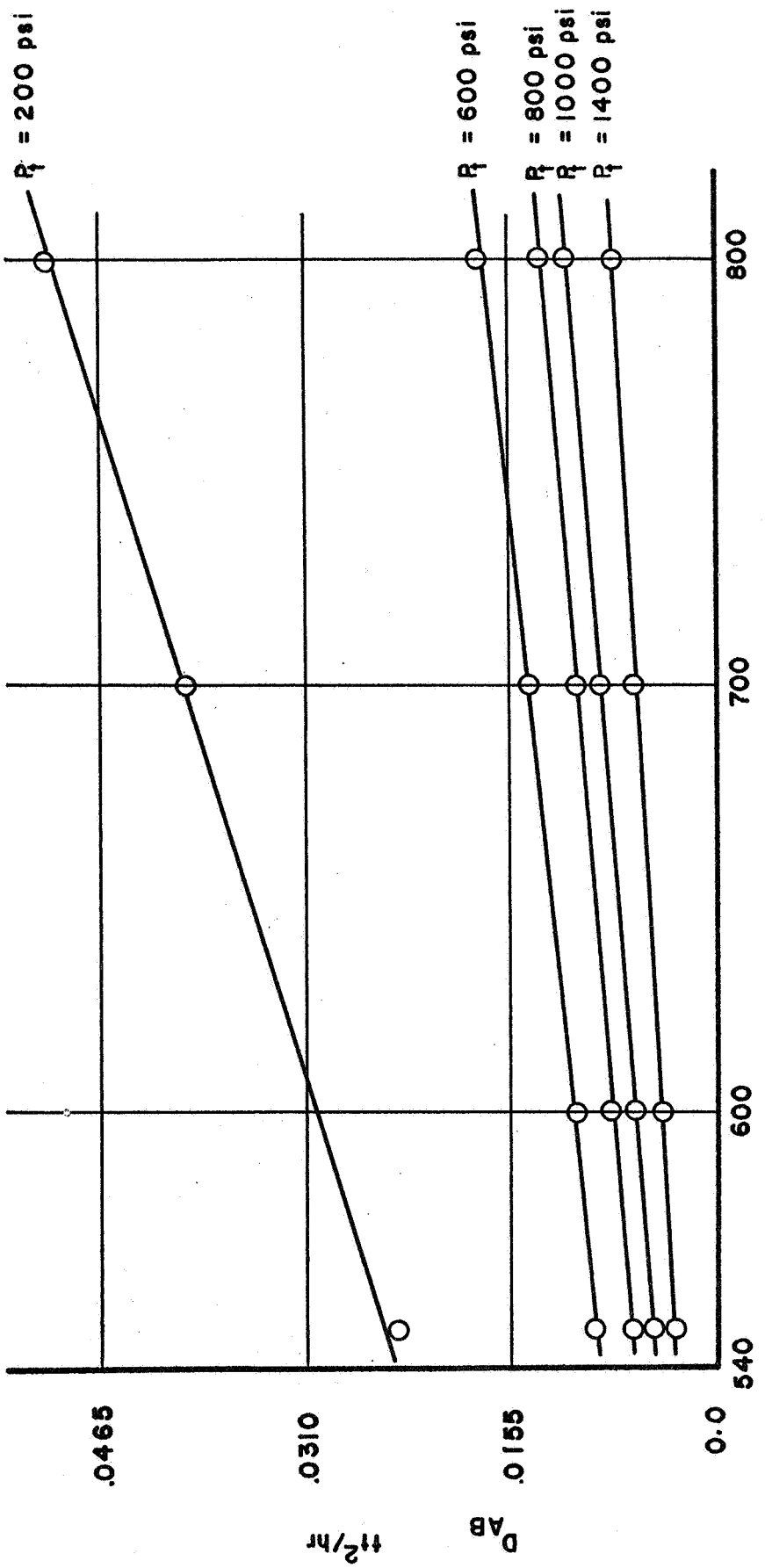

Figure 11. The binary diffusion coefficient D_{AB} for n-Pentane-Nitrogen gas system. The diffusion coefficient equation is due to Hirschfelder, Bird, and Spotz.

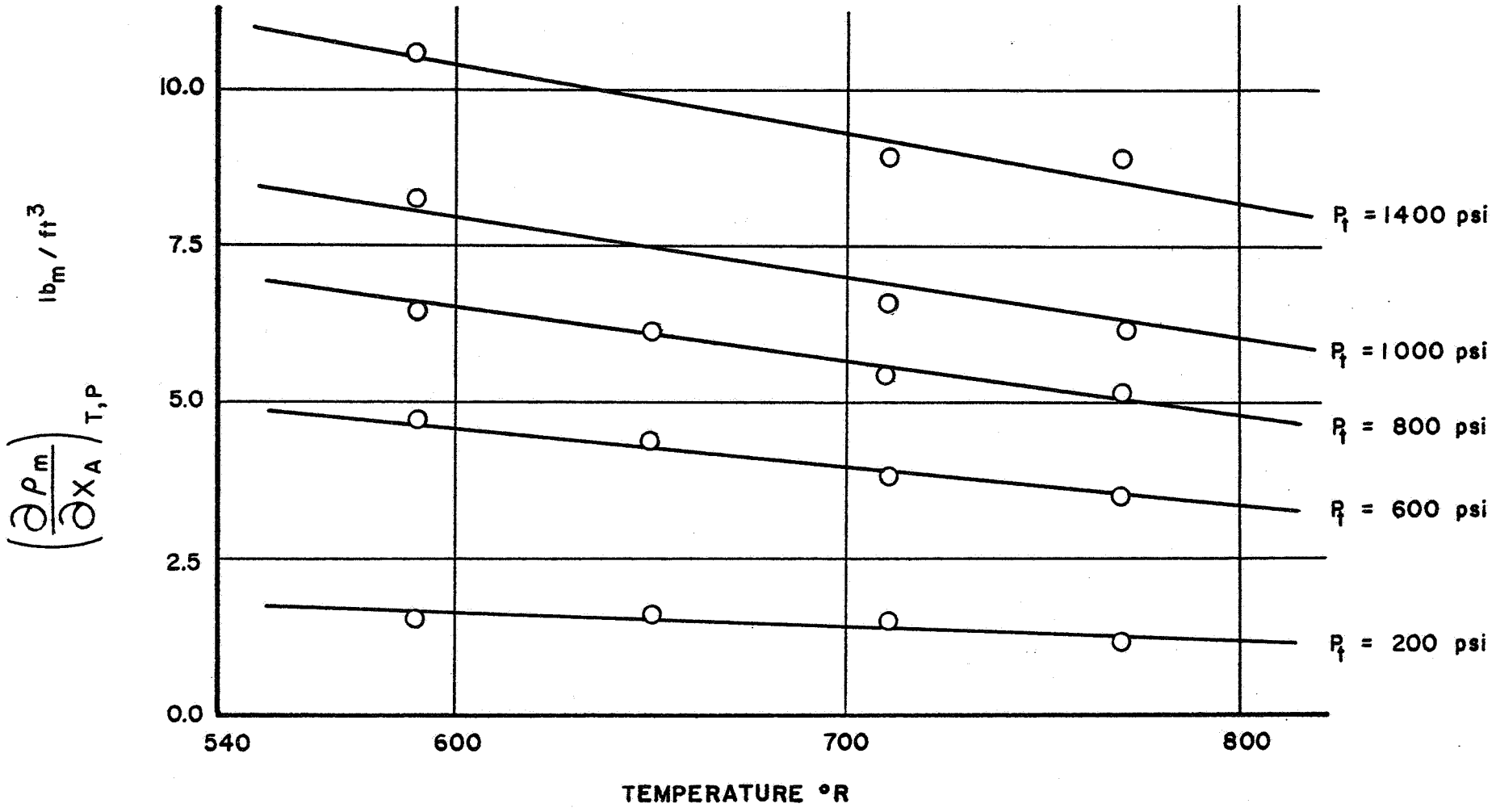

Figure 12. The change in a binary mixture density with respect to the concentration of one component as a function of temperature. The binary components are n-Pentane vapor and Nitrogen gas.

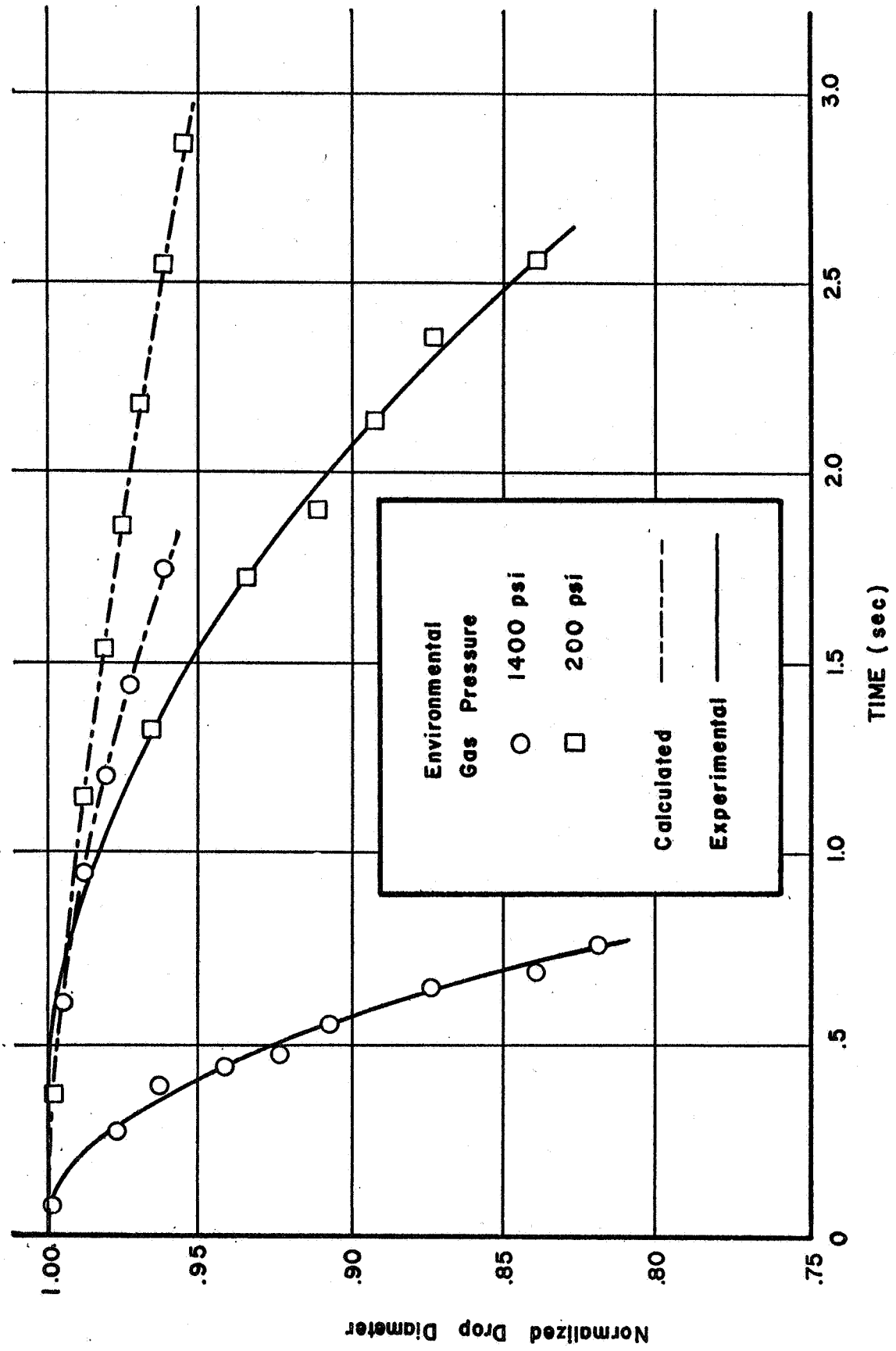

Figure 13. Experimental and Calculated Radius-time Histories for n-Pentane Drops.

TABLE I

VARIATION IN THE INITIAL TEMPERATURE AND THE INITIAL RADIUS FOR n-PENTANE DROPS VAPORIZING IN NITROGEN GAS ENVIRONMENT AT 850°R

Run	Initial Temperature		Initial Radius		
	Temperature Deviation (Rankine)	% Deviation From Mean	Radius Deviation (inches)	% Deviation From Mean	Environment Pressure (psi)
63-6	15.51	2.60%	0.0039	10.83%	200
63-3	16.89	2.90%	0.0016	4.44%	400
63-2	-13.71	2.30%	0.0013	3.61%	600
63-1	-4.71	0.82%	0.0014	3.89%	600
62-7	2.49	0.43%	0.0023	6.39%	800
62-6	11.49	1.99%	-0.0001	0.27%	800
62-5	2.49	0.43%	0.0056	15.50%	1000
62-4	-4.71	0.81%	-0.0021	5.80%	1000
62-3A	-10.11	1.75%	-0.0016	4.44%	1200
62-3B	-22.71	3.90%	-	-	1200
62-2	-13.71	2.38%	-0.0020	0.55%	1200
63-7	-4.71	0.82%	-0.0013	3.61%	1400

Mean Initial Temperature 576.1°R

Mean Initial Drop Radius 0.0360 in = 914.4μ

TABLE II

RESULTS OF THE ENERGY BALANCE ANALYSIS

Run 63-7 P_T=1400psi T_e=850°R

	h	q_T	$\frac{q_{th}}{4\pi r^2}$	q_{rad}	q_d	q_{SH}	$\%q_{th}$	$\%q_{rad}$
Sec	B/ft^2-sec-F	B/ft^2-sec	B/ft^2-sec	B/ft^2-sec	B/ft^2-sec	B/ft^2-sec		
0.25	.033	8.91	.112	.1905	6.75	2.16	1.6%	2.8%
0.50	.0476	10.87	.105	.1745	7.07	3.80	1.5%	2.5%
1.00	.0885	15.915	.1515	.1026	9.455	6.46	1.6%	1.08%

Run 63-6 P_T=200psi T_e=850°R

	h	q_T	$\frac{q_{th}}{4\pi r^2}$	q_{rad}	q_d	q_{SH}	$\%q_{th}$	$\%q_{rad}$
Sec	B/ft^2-sec-F	B/ft^2-sec	B/ft^2-sec	B/ft^2-sec	B/ft^2-sec	B/ft^2-sec		
1.00	.0088	2.710	.058	.1960	1.948	0.762	3.0%	10.0%
1.50	.01325	3.630	.057	.1890	2.180	1.450	2.6%	8.7%
2.00	.01210	3.280	.063	.1862	2.730	1.550	2.3%	6.8%

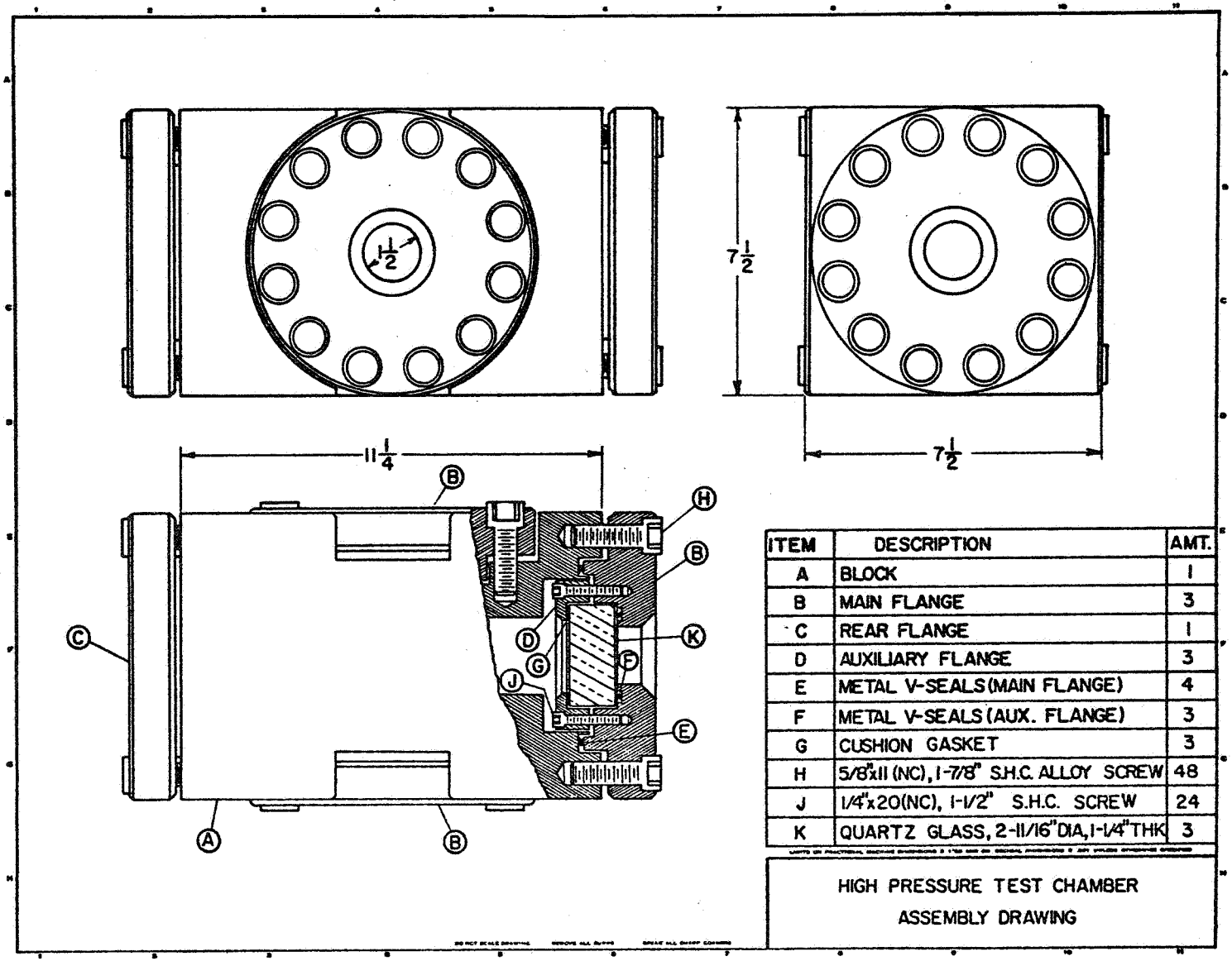

Figure 14. Assembly Drawing of the High Pressure Test Chamber.

BIBLIOGRAPHY

1. Torda, T.P., Busenberg, S., Kauffmann, J., and Steinke, R.; Rational Design Procedures for Liquid Propellant Rocket Motors; Proceedings of the Fifth International Symposium on Space Technology and Science, Tokyo 1963.

2. Priem, R.J., and Heidmann, M.F.; Propellant Vaporization As A Design Criterion For Rocket-Engine Combustion Chambers; NASA TR R-67, 1960.

3. Lambiris, S., Combs, L.P., and Levine, R.S.; "Stable Combustion Processes in Liquid Propellant Rocket Engines" Combustion and Propulsion, Fifth AGARD Colloquim: High Temperature Phenomena; The MacMillan Company, New York, 1963.

4. Priem, R.J., Heidmann, M.F., and Humphrey, J.C.; A Study of Sprays Formed by Two Impinging Jets; NACA TN 3835, 1957.

5. Bittker, D.A.; An Analytical Study of Turbulent and Mixing in Rocket Combustion; NACA TN 4321, 1958.

6. Bittker, D.A., and Brokaw, R.S.; An Estimate of Chemical Space Heat Rates in Gas-Phase Combustion with Applications to Rocket Propellants; Paper No. 824-59, American Rocket Society, 1959.

7. Torda, T.P.; Aerothermochemistry of Jet-Propulsion Liquid-Propellant Rocket Motors; Symposium on Thermodynamics of Jets and Rocket Propulsion, A.I.Ch.E., 1959.

8. Torda, T.P.; Combustion Instability of Liquid Propellant Rocket Engines -- Notes on the State of the Art and Proposed Areas of Investigations; presented to the AFAOR, Jan. 1962 Armour Research Foundation TM D-29.

9. Combs, L.P.; Calculated Propellant Droplet Heating Under F-1 Combustion Chamber Conditions; Rocketdyne RR 64-25 June 1964.

10. Wieber, P.R.; Calculated Temperature Histories of Vaporizing Droplets to the Critical Point; AIAA Journal Vol. 1, No. 12, p2764.

11. Hersch, M.; A Mixing Model for Rocket Engine Combustion; NASA TN D-2881, June 1965.

12. El Wakil, M.M., Uyehara, O.A., and Myers, P.S.; A Theoretical Investigation of the Heating-up Period of Injected Fuel Droplets Vaporizing in Air; NACA TN 3179, 1954.

13. El Wakil, M.M., Priem, R.J., Brikowski, H.J., Myers, P.S., and Uyehara, O.A.; Experimental and Calculated Temperature and Mass Histories of Vaporizing Fuel Drops; NACA TN 3490, 1955.

14. Priem, R.J.; Vaporization of Fuel Drops Including the Heating-up Period; Ph.D. Thesis, University of Wisconsin, 1955.

15. Ranz, W.E., and Marshall, W.R.; Evaporation From Drops I & II; Chemical Engineering Progress; Vol. 48, No. 3, p141 and Vol. 48, No. 4, p173.

16. Spaulding, D.B.; Theory of Partical Combustion at High Pressures; A.R.S. Journal Vol. 29, p828 1959.

17. Brzustowski, T.A.; Chemical and Physical Limits on Vapor-Phase Diffusion Flames of Droplets; Canadian Journal of Chem.Eng., Feb., 1965.

18. Wilke, C.R., and Lee, C.Y.; Estimation of Diffusion Coefficients of Gases and Vapors; Industrial and Engineering Chemistry, Vol. 47, No. 6, p1253, June 1955.

19. Campbell, D.T.; Combustion Instability Analysis at High Chamber Pressures; AFRPL-TR-67-222, August 1967.

20. Reid, R.C., and Sherwood, T.K.; The Properties of Gases and Liquids: Their Estimates and Correlation; 2nd Ed., McGraw-Hill Book Company, New York, 1966.

21. Zemansky, M.W.; Heat and Thermodynamics; 4th Ed., McGraw-Hill Book Company, New York, 1957.

22. Buddenberg, J.W., and Wilke, C.R.; Calculation of Gas Mixture Viscosities; Industrial and Engineering Chemistry, Vol. 41, No. 7, p1345, July 1949.

23. Bird, R.B., Stewart, W.E., and Lightfoot, E.N.; Transport Phenomena; John Wiley & Sons, Inc., 1960.

24. Maxwell, J.B.; Data Book on Hydrocarbons; O.Van Nostrand Co. Inc., 1950.

REPORT DISTRIBUTION LIST FOR

CONTRACT NO. NGR 14-004-006

NASA Lewis Research Center (3)
21000 Brookpark Road
Cleveland, Ohio 44135
Attention: Robert D. Ingebo

NASA Scientific and Technical
Information Facility (6)
Box 5700
Bethesda, Md.

NASA Lewis Research Center (2)
21000 Brookpark Road
Cleveland, Ohio 44135
Attention: Library

NASA Lewis Research Center
21000 Brookpark Road
Cleveland, Ohio 44135
Attention: Report Control Office

National Aeronautics and
Space Administration (10)
Washington, D.S. 20546
Attention: Office of Research
Grants and Contracts

NASA Ames Research Center
Moffett Field, Calif. 94035
Attention: Library

NASA Flight Research Center
P. O. Box 273
Edwards, Calif. 93523
Attention: Library

NASA Goddard Space Flight Center
Greenbelt, Md. 20771
Attention: Library

Jet Propulsion Laboratory
4800 Oak Grove Dr.
Pasadena, California 91103
Attention: Library

NASA Langley Research Center
Langley Station
Hampton, Va. 23365

NASA Manned Spacecraft Center
Houston, Texas 77001
Attention: Library

NASA Marshall Space Flight Center
Huntsville, Ala. 35813
Attention: Library

NASA Western Operations
150 Pico Blvd.
Santa Monica, Calif. 90406
Attention: Library

Polytechnic Institute of Brooklyn
Graduate Center
Route 110
Farmingdale, New York
Attention: V.D. Agosta

Applied Physics Laboratory
The Johns Hopkins University
8621 Georgia Avenue
Silver Spring, Maryland
Attention: W. G. Berl

Ohio State University
Rocket Research Laboratory
Department of Aeronautical and
Astronautical Engineering
Columbus 10, Ohio
Attention: L. E. Bollinger

Chemical Propulsion Information Agency
Applied Physics Laboratory
The Johns Hopkins University
8621 Georgia Avenue
Silver Spring, Maryland 20910
Attention: T. W. Christian

Multi-Tech, Inc.
Box 4186 No. Annex
San Fernando, California
Attention: F. B. Cramer

Aerospace Corporation
P. O. Box 95085
Los Angeles, California
Attention: O. W. Dykema

Space Technology Lab., Inc.
5740 Arbor Vitae
Los Angeles, California
Attention: G. W. Elverum

Rocketdyne
Div. of North American Aviation
6633 Canoga Avenue
Canoga Park, California
Attention: R. Fontaine

Dynamic Science Corporation
1445 Huntington Drive
South Pasadena, California
Attention: M. Gerstein

NASA
Headquarters
6th & Independence Avenue, S.W.
Washington, D.C. 20546
Attention: A. Gessow

Princeton University
Forrestal Research Center
Princeton, New Jersey
Attention: I. Glassman

Defense Research Corporation
P. O. Box 3587
Santa Barbara, California
Attention: B. Gray

RTNT
Bolling Field
Washington, D.C. 20332
Attention: L. Green, Jr.

Princeton University
Forrestal Research Center
Princeton, New Jersey
Attention: D. T. Harrje

Aerojet-General Corporation
P. O. Box 1947
Sacramento, California 95809
Attention: R. J. Hefner

Department of the Navy
Office of Naval Research
Washington, D. C. 20360
Attention: R. O. Jackel

Rocketdyne
Div. of North American Aviation
6633 Canoga Avenue
Canoga Park, California
Attention: R. B. Lawhead
Attention: R. S. Levine

Pratt & Whitney Aircraft Co.
West Palm Beach, Florida
Attention: G. Lewis

Thiokol Chemical Corporation
Reaction Motors Division
Denville, New Jersey
Attention: D. Mann

University of Wisconsin
Dept. of Mechanical Engineering
1513 University Avenue
Madison, Wisconsin 53705
Attention: P. S. Myers

Dartmouth University
Hanover, New Hampshire
Attention: P. D. McCormack

University of Michigan
Aeronautical & Astronautical
Engineering Laboratories
Aircraft Propulsion Laboratory
North Campus
Ann Arbor, Michigan
Attention: J. A. Nicholls

Institute of Engineering Research
University of California
Berkeley, California
Attention: A. K. Oppenheim

Purdue University
School of Mechanical Engineering
Lafayette, Indiana
Attention: J. R. Osborn

United Technology Center
Div. of United Aircraft Corporation
Sunnyvale, California
Attention: R. H. Osborn

NASA Lewis Research Center
21000 Brookpark Road
Cleveland, Ohio 44135
Attention: R. J. Priem

Aerojet-General Corporation
P. O. Box 1947
Sacramento, California 95809
Attention: F. H. Reardon

Bell Aerosystems Corporation
P. O. Box 1
Buffalo, New York
Attention: T. Rossman

ARL (ARC)
Bldg. 450
Wright-Patterson AFB
Dayton, Ohio
Attention: K. Scheller

Aerospace Corporation
P. O. Box 95085
Los Angeles, California
Attention: W. C. Strahle

NASA
Headquarters
6th & Independence Avenue, S.W.
Washington, D. C. 20546
Attention: A. O. Tischler

Geophysics Corporation of America
Technical Division
Bedford, Massachusetts
Attention: A. C. Toby

Masaachusetts Institute of Technology
Department of Mechanical Engineering
Cambridge 39, Massachusetts
Attention: T. Y. Toong

Warner-Swasey Company
Control Instrument Division
32-16 Downing Street
Flushing, New York 11354
Attention: R. H. Tourin

Pratt & Whitney Aircraft Company
Div. of United Aircraft Corporation
Engineering, Bldg. 1-F
East Hartford, Connecticut
Attention: D. H. Utvik

NASA Lewis Research Center
21000 Brookpark Road
Cleveland, Ohio 44135
Attention: E. Conrad

Naval Ordnance Test Station
China Lake, California 93557
Attention: E. W. Price

NASA Marshall Space Flight Center
Huntsville, Alabama 35812
Attention: R. J. Richmond
R-P&VE-PAC

Director
Jet Propulsion Laboratory
California Institute of Technology
Pasadena, California
Attention: J. H. Rupe

NASA Manned Spacecraft Center
Houston, Texas 77001
Attention: J. G. Thibodaux
Code EP

Air Force Rocket Propulsion Lab.
Edwards, California 93523
Attention: R. R. Weiss RPRR

U. S. Army Missile Command
Redstone Arsenal
Huntsville, Alabama
Attention: W. W. Wharton, AMSMI-RRK

Air Force Office of Scientific Research
Propulsion Division
Washington, D. C.
Attention: B. T. Wolfson